THE JOURNAL OF BIOLOGICAL CHEMISTRY VOL. 283, NO. 50, pp. 35164–35172, December 12, 2008

The Structure of the Glial Cell Line-derived Neurotrophic Factor-Coreceptor Complex

*INSIGHTS INTO RET SIGNALING AND HEPARIN BINDING**[S]

Received for publication, April 2, 2008, and in revised form, October 6, 2008 Published, JBC Papers in Press, October 8, 2008, DOI 10.1074/jbc.M802543200

Vimal Parkash[‡], Veli-Matti Leppänen[‡1], Heidi Virtanen[‡], Jaana M. Jurvansuu[‡], Maxim M. Bespalov[‡], Yulia A. Sidorova[‡], Pia Runeberg-Roos[‡], Mart Saarma[‡], and Adrian Goldman[‡§2]

From the [‡]Institute of Biotechnology and the [§]Neuroscience Center, University of Helsinki, FIN-00014 Helsinki, Finland

Glial cell line-derived neurotrophic factor (GDNF), a neuronal survival factor, binds its co-receptor GDNF family receptor α1 (GFRα1) in a 2:2 ratio and signals through the receptor tyrosine kinase RET. We have solved the $GDNF_2$·$GFR\alpha1_2$ complex structure at 2.35 Å resolution in the presence of a heparin mimic, sucrose octasulfate. The structure of our $GDNF_2$·$GFR\alpha1_2$ complex and the previously published $artemin_2$·$GFR\alpha3_2$ complex are unlike in three ways. First, we have experimentally identified residues that differ in the ligand-GFRα interface between the two structures, in particular ones that buttress the key conserved $Arg^{GFR\alpha}$-Glu^{ligand}-$Arg^{GFR\alpha}$ interaction. Second, the flexible GDNF ligand "finger" loops fit differently into the GFRαs, which are rigid. Third, and we believe most importantly, the quaternary structure of the two tetramers is dissimilar, because the angle between the two GDNF monomers is different. This suggests that the RET-RET interaction differs in different $ligand_2$-co-$receptor_2$-RET_2 heterohexamer complexes. Consistent with this, we showed that $GDNF_2$·$GFR\alpha1_2$ and $artemin_2$·$GFR\alpha3_2$ signal differently in a mitogen-activated protein kinase assay. Furthermore, we have shown by mutagenesis and enzyme-linked immunosorbent assays of RET phosphorylation that RET probably interacts with GFRα1 residues Arg-190, Lys-194, Arg-197, Gln-198, Lys-202, Arg-257, Arg-259, Glu-323, and Asp-324 upon both domains 2 and 3. Interestingly, in our structure, sucrose octasulfate also binds to the Arg^{190}-Lys^{202} region in GFRα1 domain 2. This may explain how GDNF·GFRα1 can mediate cell adhesion and how heparin might inhibit GDNF signaling through RET.

GDNF,[3] originally characterized as a growth factor promoting the survival of midbrain dopaminergic neurons (1), regulates the differentiation and development of many peripheral neurons (2) and is neuroprotective (3). GDNF is also a morphogenic factor in kidney and spermatogonia development (reviewed by Airaksinen and Saarma (2)). Some clinical trials have indicated that perfusing GDNF into the putamen may be therapeutically beneficial in Parkinson disease (4). These neuroprotective and therapeutic roles have generated wide interest in the study of the GDNF signaling system.

There are three other GDNF family ligands (GFLs), neurturin (NRTN (5)), artemin (ARTN (6)), and persephin (PSPN (7)), and knock-out mice experiments have made it clear that the order of biological importance is GDNF ≫ NRTN > ARTN > PSPN (2). They all signal primarily through the receptor tyrosine kinase RET (8). The extracellular region of RET has four cadherin-like domains and a cysteine-rich domain. Mutations in RET can cause both gain-of-function and loss-of-function diseases. In the former category are hereditary medullary thyroid carcinoma and multiple endocrine neoplasias of types 2A and 2B (9, 10), whereas Hirschsprung disease is an example of the latter (10).

GFLs are distant relatives of transforming growth factor β (2). Each GFL has its own co-receptor α: GDNF requires GFRα1; NRTN requires GFRα2; ARTN requires GFRα3; and PSPN requires GFRα4 (2). The GFRαs, which are glycosylphosphatidylinositol-anchored to the cell surface, typically have three homologous cysteine-rich domains with C-terminal extensions of various lengths (11, 12). Domain 2 (D2) clearly binds the GFL (13–15). The roles of domain 1 (D1) and domain 3 (D3) are less certain, but D1 is not necessary for RET binding GFRα1 (16) and is absent in GFRα4 (11). Many models have been proposed for the RET activation mechanism because of the requirement for a RET_2·$GFR\alpha_2$·GFL_2 heterohexamer. The $ARTN_2$·$GFR\alpha3_2$ (13) structure is symmetric, consistent with the idea (17) that a dimeric GFL first binds two molecules of GFRα, which then interacts with and dimerizes RET. Schlee *et al.* (18) have recently shown that ARTN first binds to a monomer of GFRα3, followed by sequential recruitment of one RET molecule and then additional molecules of GFRα3 and RET.

* This work was supported by Academy of Finland Grants 1111771 and 1114752 (to A. G.), 70891 (to V.-M. L.), and 1105237 and 1109071 (to M. S.) and by grants from the Sigrid Jusélius Foundation (to A. G. and M. S.), Biocentrum Helsinki (to A. G. and M. S.), and the Neuroscience Centre (to A. G.). The costs of publication of this article were defrayed in part by the payment of page charges. This article must therefore be hereby marked "*advertisement*" in accordance with 18 U.S.C. Section 1734 solely to indicate this fact.

The atomic coordinates and structure factors (code 2v5e) have been deposited in the Protein Data Bank, Research Collaboratory for Structural Bioinformatics, Rutgers University, New Brunswick, NJ (http://www.rcsb.org/).

[S] The on-line version of this article (available at http://www.jbc.org) contains supplemental Fig. 1.

[1] Present address: Molecular Cancer Biology Laboratory, Biomedicum Helsinki, Haartmaninkatu 8, University of Helsinki, FIN-00014 Helsinki, Finland.

[2] To whom correspondence should be addressed: Research Program for Structural Biology and Biophysics, Institute of Biotechnology, Biocenter 3, University of Helsinki, Viikinkaari 1, FIN-00014 Helsinki, Finland. Tel.: 358-9-191-58923; Fax: 358-9-191-59940; E-mail: adrian.goldman@helsinki.fi.

[3] The abbreviations used are: GDNF, glial cell-line derived neurotrophic factor; NRTN, neurturin; ARTN, artemin; PSPN, persephin; GFLs, GDNF family ligands; GFRα, GDNF family receptor α; ELISA, enzyme-linked immunosorbent assay; MAPK, mitogen-activated protein kinase; SOS, sucrose octasulfate.

GDNF in complex with GFRα1 can also signal through the neural cell adhesion molecule independent of RET (19), and recent studies suggest that the $GDNF_2$·$GFR\alpha1_2$ complex can also act as an adhesin, mediating cell-cell interactions (20). Furthermore, the N terminus of GDNF has been shown to bind heparin (21). Understanding the structure of the $GDNF_2$·$GFR\alpha1_2$ complex may thus give insight into the various ways in which GDNF is involved in development and maintenance of neuronal and other cells.

We present here the crystal structure of the $GDNF_2$·$GFR\alpha1_2$ complex in the presence of a heparin mimic, sucrose octasulfate (SOS). Structural, mutagenesis, and biochemical studies have allowed us to understand the structural basis for ligand binding specificity. We have been able to identify the putative RET-binding site on GFRα1 and to understand the structural basis for differential GFL signaling. Finally, our structure also suggests how $GDNF_2$-$GFR\alpha1_2$ interactions might lead to cell-cell adhesion and RET-independent signaling.

MATERIALS AND METHODS

Expression and Purification of the $GDNF_2$·$GFR\alpha1_2$ Complex—The numbering of the amino acid residues of rat GFRα1 refers to SwissProt accession number Q62997. Primers included a His_6 tag, followed by a thrombin cleavage site for the truncated rat GFRα1 construct, residues 145–425. We did not add His_6 tag to the mature human GDNF construct (GenBank™ ID AH003115, excluding the 77-residue preprosequence), numbered 1–134. We used human, not rat, GDNF, since in the 34–134 region there are just six changes, the only nonconservative one being Met → Thr at residue 78. Both constructs were cloned into baculovirus vector pK503.9 (22), a pFastBac derivative (Invitrogen), which added a FLAG tag and an insect cell secretion signal sequence to the N terminus.

High titer GDNF and GFRα1 baculovirus stocks grown in Sf9 cells were used at a 1:1 ratio to infect Tn5 cells for the co-expression of the protein complex. Cells were grown in serum-free HyQ-SFX medium (HyClone) supplemented with 50 μg/ml gentamycin (Sigma) at +27 °C. Three days after co-infection, the supernatant was harvested by centrifugation to remove cellular material. Tangential flow concentration was used to concentrate the supernatant and to change the buffer to phosphate-buffered saline, pH 7.4. The $GDNF_2$·$GFR\alpha1_2$ complex was purified by adding Ni^{2+}-resin (Ni^{2+}-charged chelating Sepharose; GE Healthcare) to the concentrated supernatant in batch. After a 45-min incubation at +4 °C, the resin was washed with phosphate-buffered saline in the presence of 10 mM imidazole, and the complex was eluted with 500 mM imidazole in phosphate-buffered saline, pH 8.0. To remove the His tag, the buffer was adjusted to phosphate-buffered saline with spin concentrators, and the complex was incubated overnight at room temperature with 10 units of thrombin (GE Healthcare)/mg of the complex. Two millimolar SOS was added to the protein solution before gel filtration. Finally, the complex was purified by gel filtration on a Superdex 200 (GE Healthcare) column in HEPES-buffered (pH 7.5) 0.3 M NaCl and visualized on SDS-PAGE to check that a complex had formed (Fig. 1*A*).

Site-directed Mutagenesis—The mutant clones of GFRα1 were constructed using the QuikChange (Stratagene) site-directed mutagenesis protocol. The constructs were transformed into DH5α cells, and the transformed cells were selected on LB/ampicillin agar plates. The mutated plasmids were used for cloning into baculovirus. All clones were sequenced to ensure that no undesired mutations were introduced during PCR.

RET Activation and ELISA—RET phosphorylation assays were done in MG87RET cells, derived from the mouse NIH 3T3 cells, which are stably transfected with RET but do not express GFRα1 (23). MG87RET cells were starved for 4 h in serum-free Dulbecco's modified Eagle's medium at 37 °C and subsequently stimulated for 60 min at 37 °C by adding 1 μg/ml soluble wild-type GFRα1 D23C or mutant GFRα1 D23C (Fig. 1*B*) with or without 100 ng/ml GDNF. After lysis with lysis buffer (Tris-buffered saline, 1% Triton X-100, 1% Nonidet P-40, 10% glycerol, 2 mM EDTA, 1 mM Na_3VO_4, Complete Mini protease inhibitor from Roche Applied Science), the lysates were centrifuged in a tabletop centrifuge, at 10,000 rpm for 10 min to pellet the nuclei. The cleared lysates were applied to a 96-well plate (OptiPlate 96 F HB, Black; Wallac), which had been previously coated with 0.5 μg/ml RET C-20 antibody (Santa Cruz Biotechnology) and blocked with 2% bovine serum albumin in Tris-buffered saline, and the plate was incubated at +4 °C for 1 h. Phosphorylated RET was detected using anti-phosphotyrosine antibodies (4G10; 1:1000 dilution; Upstate Biotechnology), anti-mouse horseradish peroxidase-conjugated antibodies (1:3000 dilution; DAKO A/S), and the enhanced chemiluminescence reaction (Femto ELISA ECL kit; Pierce). All washes between the incubations were done with the same washing buffer (Tris-buffered saline, 1% Triton X-100). Signal detection was done using a MicroBeta luminometer (PerkinElmer Life Sciences). The ELISA-based assay was more sensitive and had a much wider dynamic range than our previous Western blot assay (14), because GFRα1 was separately expressed in baculovirus/insect cells and was added as a soluble component.

MAPK Activity Assay—MG87RET cells were transfected with the MAPK activation detection system (Gal4-ELK plasmid and G4-Luc plasmid (6), a kind gift of Prof. J. Milbrandt) and plasmids expressing either rat GFRα1 or human GFRα3 (also from Prof. J. Milbrandt). Stably transfected cells were selected in the presence of 750 and 500 μg of Geneticin/ml of growth medium, respectively. After selection, cells were cultivated in the culture medium (Dulbecco's modified Eagle's medium, 10% fetal bovine serum, normocin, 2 μg/ml puromycin, 500 μg/ml Geneticin, 15 mM HEPES, pH 7.2).

Six hours before the assay, cells were plated on 96-well plates at a cell density of 400,000 cells/ml. GDNF or ARTN was diluted in growth medium without selective antibiotics to a final concentration of 100 ng/ml and added to the cells for varying lengths of time. After incubation with the neurotrophic factors, the cells were washed once with culture medium and left for 24 h in the incubator to produce luciferase, followed by the addition of the cell lysis reagent (Promega) (20 μl/well). Cells were incubated on a rotary shaker for 15 min and then subjected to one freeze-thaw cycle to ensure complete lysis. To measure luciferase activity, 5 μl of lysate was added to 20 μl of luciferase assay reagent (Promega) and counted on a MicroBeta luminometer (PerkinElmer Life Sciences).

Heparin Affinity Chromatography—The baculovirus expression system was used to produce full-length GFRα1 as well as GFRα1 D23C (14). The recombinant GFRαs had N-terminal FLAG-His_6 tags. Conditioned Sf9 culture supernatants (10 ml) were mixed with an equal volume of 40 mM sodium phosphate buffer (pH 7.0) and then applied to a 5-ml HiTrap Heparin column (GE Healthcare) at a flow rate of 1 ml/min. After a 10-ml wash step with 20 mM sodium phosphate buffer (pH 7.0, 150 mM NaCl), we applied a linear gradient of NaCl in the same buffer up to a final concentration of 2.0 M. One-milliliter fractions were collected and immunoblotted with anti-FLAG (M1; Sigma) antibodies as well as assayed for GDNF binding activity by a scintillation proximity assay. Scintillation proximity assay polyvinyltoluene beads precoated with anti-mouse antibodies (GE Healthcare) were used together with anti-FLAG antibodies and ^{125}I-labeled GDNF, as described (14).

Crystallography—Protein complex that had been purified by size exclusion chromatography (Fig. 1*A*) was deglycosylated with peptide:*N*-glycosidase F (New England Biolabs). The buffer was then changed to 10 mM HEPES (pH 7.5) supplemented with 150 mM NaCl, 0.01% (v/v) P8340 protease inhibitor mixture (Sigma), 0.001% NaN_3, and the complex was crystallized at +4 °C using the Helsinki robot crystallization facility. The reservoir solution was 100 mM HEPES, pH 7.5, 10% polyethylene glycol 8000, 8% ethylene glycol, and the 200-nl drops were prepared by mixing 100 nl of the reservoir solution with 100 nl of the protein solution at 3 mg/ml. For data collection at −80 °C, the crystal was frozen in liquid nitrogen with the well solution containing 20% (v/v) glycerol. A full data set to 2.35 Å resolution was collected using the ID14-EH2 beamline at ESRF (Grenoble, France) (Table 1). Diffraction data were processed using XDS (24) in space group C2 (Table 1).

A single GFRα1 co-receptor and one GDNF monomer together gave a Matthews coefficient (V_M) of 2.35 Å^2/Da with 48% solvent content, suggesting that there was only a half of the quaternary complex per asymmetric unit. The other half of the complex is formed by the crystallographic 2-fold symmetry about the unique axis. We solved the structure by molecular replacement using the human GFRα3 domains 2 and 3 from the $ARTN_2$·$GFR\alpha3_2$ complex structure (Protein Data Bank code 2GH0 (13)) and rat GDNF (Protein Data Bank code 1AGQ (25)) as search models with Phaser (26). The initial *R*-factor after molecular replacement and one round of rigid body refinement was 48.5 (R_{free} 47%).

After 10 cycles of automated model building using ArpWarp (27), 69% of the residues had been built, and Refmac5 (28) refinement resulted in an initial R_{work} of 20% (R_{free} = 31%). Iterative model building and refinement using Coot (29) and Refmac5 gave a final model with R_{work} 18.4% (R_{free} = 23.7%). Individual isotropic B factors were refined using restrained refinement. Water molecules were added with Coot (29) to peaks above 3.5σ in the $F_o - F_c$ difference electron density map if they had suitable hydrogen bonding geometry and eliminated if they refined to a *B*-factor of greater than 70. The electron density quality was good throughout both the GDNF and GFRα1 structures (supplemental Fig. 1*A*) and more than 90% of residues were in the most favored regions of the Ramachandran plot (30) (Table 1). The first five residues of GFRα1 were disordered. The flexible N-terminal region of GDNF and the GFRα1 C-terminal extension (76 residues) were not visible due to proteolytic cleavage, as shown by SDS-PAGE of the crystals (data not shown). The ligand library for SOS and *N*-acetylglucosamine was generated with PRODRG (31). We validated the model using tools in Coot (29) and PROCHECK (30). Structural alignments were done using Coot (29) and PyMol (32), and sequence alignments were done using ClustalW (33).

RESULTS

Biochemical and Structural Characterization of $GDNF_2$·$GFR\alpha1_2$ Complex—We co-expressed GFRα1 domain 2–3-C (GFRα1 D23C) with GDNF in Tn5 insect cells and purified the $GDNF_2$·$GFR\alpha1_2$ complex in two steps: Ni^{2+}-Sepharose affinity purification in batch followed by size exclusion chromatography. SDS-PAGE showed that fraction 6 from the gel filtration column, which ran at about 100 kDa, contained two proteins, one of molecular mass 38 kDa (GFRα1 D23C) and the other of molecular mass 22 kDa (GDNF) (Fig. 1*A*). The crystal structure was solved by molecular replacement and refined using standard techniques (see "Materials and Methods") to R_{work} 18.4% (R_{free} 23.7%), and the final model contained residues 150–349 of GFRα1 and residues 34–134 of GDNF (Table 1).

Overview of the $GDNF_2$·$GFR\alpha1_2$ Complex and the Ligand Co-receptor Interface—In the $GDNF_2$·$GFR\alpha1_2$ complex, each GDNF monomer of the cysteine-linked homodimer, with two β-stranded finger loops and a helical heel (supplemental Fig. 1*B*), binds GFRα1 on its finger domain (Fig. 2*A*). As expected from sequence analysis and the $ARTN_2$·$GFR\alpha3_2$ structure (13) (Fig. 2*B*), GFRα1 D2 and D3 are both "triangular helix spiral" domains (14) (Fig. 2*A*). The two domains of GFRα1 pack so that D3 stabilizes D2, which in turn binds GDNF (Fig. 2*A*).

One *N*-acetylglucosamine molecule is covalently linked to GDNF N49, and an SOS molecule binds to domain 2 in GFRα1 (Fig. 2*A*). Through a crystal contact, SOS also binds to the N terminus of a symmetry-related GDNF.

At the GDNF·GFRα1 interface, the GDNF fingertips interact with the GFRα1 D2 through the center of the triangular helix spiral formed by α-helices α1, α2, and α5 (supplemental Fig. 1*B*). The GDNF·GFRα1 interface is composed of 14 contact residues from GDNF and 18 from GFRα1 D2 (Table 2), burying ~950 Å^2 as calculated with POPScomp (34). As in the ARTN·GFRα3 complex (13), the center of the interface is the Arg-171$^{GFR\alpha1}$-Glu-61^{GDNF}-Arg-224$^{GFR\alpha1}$ ion triple (Fig. 2*C*). Asn-162$^{GFR\alpha1}$ is very important (see below) in stabilizing the ion triple. The amide C=O positions the Arg-171$^{GFR\alpha1}$ guanidine group, whereas the amide -NH_2 positions Glu-61^{GDNF} by forming three hydrogen bonds, to the Glu-62^{GDNF} and Ser-112^{GDNF} backbone carbonyls and to the carboxylate side chain of Glu-61^{GDNF} (Fig. 2*C*). The key hydrophobic interactions are on the other side of Arg-171$^{GFR\alpha1}$ from Asn-162$^{GFR\alpha1}$; Tyr-120^{GDNF} packs between Ile-175$^{GFR\alpha1}$ and Leu-114^{GDNF}, and Ile-122^{GDNF} packs between Ile-175$^{GFR\alpha1}$ and Thr-176$^{GFR\alpha1}$ (Table 2 and Fig. 2*C*).

Finally, we identified two ionic interactions at the edge of the interface: the ion pair Glu-62^{GDNF}-Lys-159$^{GFR\alpha1}$ and the ion triple Asp-108^{GDNF}-Lys-168$^{GFR\alpha1}$-Asp-109$^{GFR\alpha1}$.

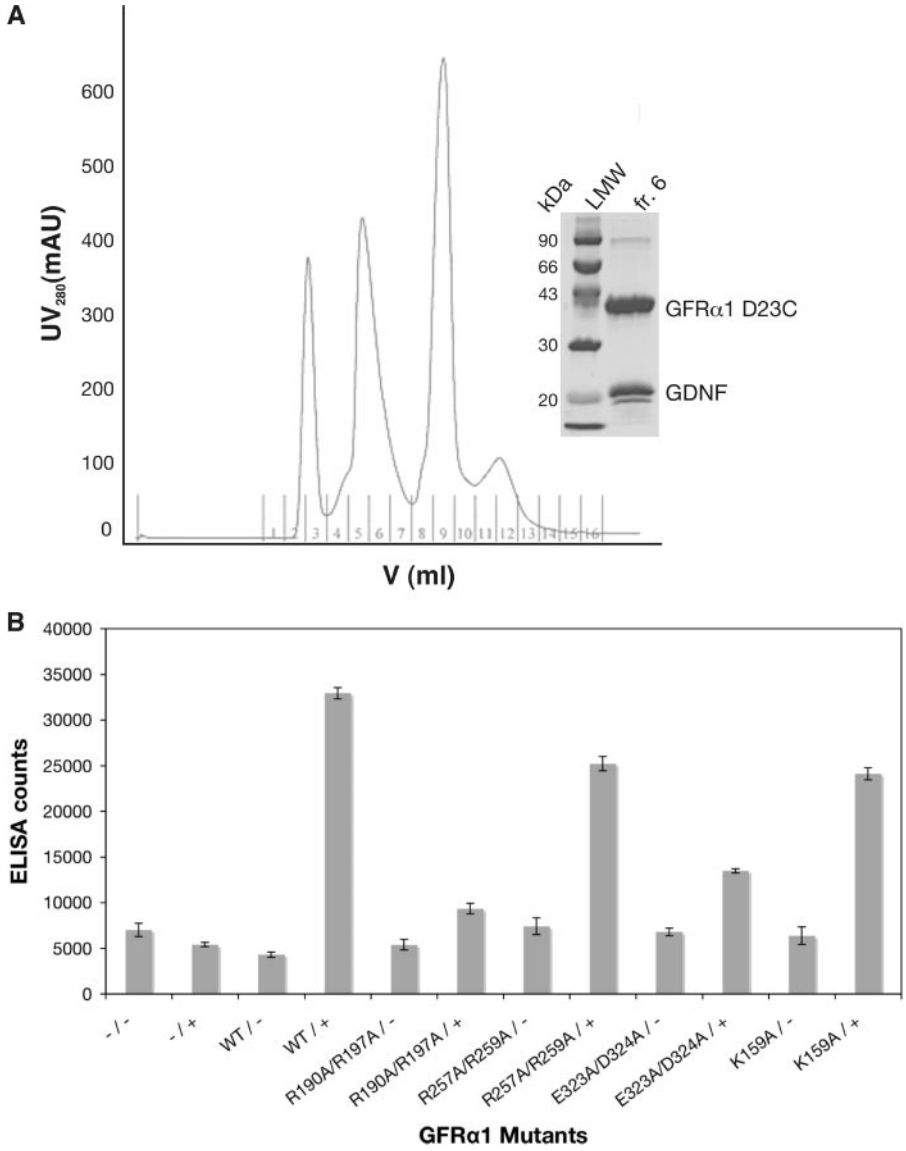

FIGURE 1. **Purification and biochemical analysis of the $GDNF_2$·$GFR\alpha1_2$ complex.** *A*, chromatogram of the purification of the $GDNF_2$·$GFR\alpha1_2$·SOS_2 complex by size exclusion chromatography. Fraction 3 is a high molecular weight aggregate, fraction 6 contains the $GDNF_2$·$GFR\alpha1_2$ complex, and fraction 9 contains the excess GFRα1 D23C (GFRα1 D23C was expressed in excess to GDNF). *Inset*, SDS-PAGE shows low molecular weight (*LMW*) marker in *lane 1* and fraction 6 in *lane 2*. mAu, milli absorption unit. *B*, ELISA studies of RET phosphorylation in MG87RET cells in the presence of wild type or various GFRα1 D23C mutants. Negative controls were as follows: −/−, neither GFRα1 nor GDNF added; −/+, only GDNF added. We measured the stimulation by GDNF by performing the experiments in the absence (−) and presence (+) of GDNF with at least four replicates per experiment. *Error bars*, S.E. of five readings. *WT*, wild type.

Heparin Binding Studies—The heparin mimic sucrose octasulfate (SOS) binds to and co-purifies with the $GDNF_2$·$GFR\alpha1_2$ complex over the gel filtration column. The negatively charged sulfate groups bind to Arg-190, Lys-194, Arg-197, Gln-198, and Lys-202 on GFRα1 D2 and to Asn-253, Tyr-254, and Arg-259 in the α6-α7 turn of GFRα1 D3 (Fig. 3*A*). SOS also mediates a crystal contact with GDNF in the neighboring complex. It binds Arg-35, Lys-37, and Arg-39 in the GDNF heel region (Fig. 3*B*), consistent with recent biochemical studies (21).

The heparin-binding properties of the full-length GFRα1 and GFRα1 D23C were also tested with a heparin column (Fig. 3*C*). The full-length GFRα1 eluted only at very high (>1 M) NaCl concentration, indicating strong binding. GFRα1 D23C eluted at about half of the concentration, suggesting reduced but still specific binding. These results and the presence of SOS in the crystal structure are consistent with earlier suggestions that the Arg-190 to Lys-202-positive patch in GFRα1 D2 might bind heparan sulfate (14, 35). This could explain why exogenous heparin can inhibit RET signaling (35) if RET also binds to the same region.

Mutagenesis and Binding Studies—We made a series of mutants, which fell into three categories: mutants in the GDNF·GFRα1 interface (K159A, N162A, K168A, and I175G); mutants in the "SOS-binding" region (R190A/R197A, K194A, Q198A/K202A, and R257A/R259A); and "RET-binding" residues (13) (D164A, R257A/R259A, and E323A/D324A) (supplemental Fig. 1*C*). The first category probes specific details of the GDNF·GFRα1 interface to try to gain a fuller understanding of what aspects of the interface are important for specificity; the second category tests if the SOS-binding region is important for RET and/or heparin binding; and the third examines the region predicted by Wang *et al.* (13) to bind RET (supplemental Fig. 1*C*). In addition, we tested two mutations outside these regions: R217E, which had appeared to show some allosteric effects (14), and R240A, on the opposite side of the GFRα1 to the SOS-binding surface. We used MG87RET cells (expressing RET) and detected the RET tyrosine phosphorylation by ELISA.

The mutations N162A and I175G in the key buttressing interactions in the center of the GDNF·GFRα1 interface caused the largest changes (more than 95% reduction with respect to wild type) in RET phosphorylation (Table 3). Mutations to peripheral residues in the GDNF-binding interface, such as K159A and K168A, reduced phosphorylation much less (60 and 35% as active as wild type (Table 3 and Fig. 1*B*)). The effect of the D164A mutant was also very small, suggesting that Asp-164 is not important. The changes in IC_{50} as measured by scintillation proximity assay with ^{125}I-labeled GDNF were consistent with these results.[4]

[4] M. M. Bespalov, unpublished results.

TABLE 1
X-ray data collection and refinement statistics

Parameter	Value
Data collection	
Resolution range (Å)[a]	20 to 2.35 (2.45 to 2.35)
Space group	C2
Unit cell (Å)	$a = 58.9$, $b = 75.7$, $c = 105.5$, $\beta = 91.9$
Wavelength (Å)	0.933
Molecules/Asymmetric unit	1
No. of reflections	
Total	68,591
Unique	19,071
Completeness (%)[a]	98.2 (87.0)
I/σ^a	16.0 (4.29)
R_{sym} (%)[a]	6.4 (23.0)
Refinement	
Resolution range (Å)	20 to 2.35
Reflections	18,089
R_{work} (%)	18.4
R_{free} (%)	23.7
Average *B*-factor (Å^2)	
Protein (2356 atoms)	26.6
SOS (55 atoms)	27.4
N-Acetylglucosamine (14 atoms)	47
1,2-Ethanediol (16 atoms)	37
Solvent (223 atoms)	29.5
Root mean square deviation from ideal values	
Bond lengths (Å)	0.01
Angles (degrees)	1.25
Ramachandran plot	GFRα1, GDNF
Most favored (%)	91.3, 92.3
Additionally allowed (%)	8.7, 7.7

[a] Values in parentheses indicate the statistics in the highest resolution shell.

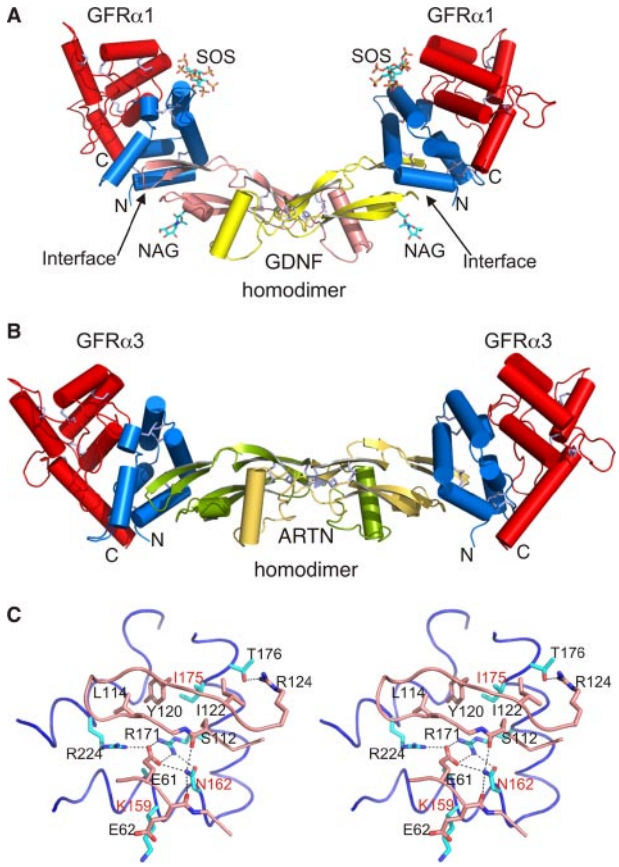

FIGURE 2. **The $GDNF_2$·$GFR\alpha1_2$ heterotetrameric complex and the GDNF-GFRα1 interface.** *A*, overall view of the $GDNF_2$·$GFR\alpha1_2$·SOS_2 complex viewed with the 2-fold axis *vertical*. The cell membrane surface would be *below* in this orientation. The GDNF monomers are *colored yellow* and *salmon*, the GFRα1 D2s are *blue*, and the GFRα1 D3s are *red*. The helices are shown as *cylinders*, and β-strands are shown as *arrows*. SOS and *N*-acetylglucosamine (*NAG*) are shown as *sticks* in *atom coloring* (*yellow*, sulfur; *red*, oxygen; *blue*, nitrogen; *cyan*, carbon). Disulfide bridges are shown in *light blue sticks*. *B*, overall view of the $ARTN_2$·$GFR\alpha3_2$ complex (Protein Data Bank code 2GH0 (13)), viewed at the same scale and in the same schematic diagram and orientation as $GDNF_2$·$GFR\alpha1_2$ in Fig. 2*A*. The ARTN monomers are *pea green* and *light yellow*, the GFRα3 D2s are *blue*, and the GFRα3 D3s are *red*. *A* and *B* emphasize the difference in bend angle between the two complexes (see "Results" for details). Since the scale (not shown) is the same, it is clear that the $GDNF_2$·$GFR\alpha1_2$ heterotetramer is the more compact of the two complexes. *C*, close-up view of the GDNF·GFRα1 interface in stereo, showing the interface residues as *sticks*, *color-coded* by atoms (*red*, oxygen; *blue*, nitrogen; *cyan*, carbon (GFRα1); *salmon*, carbon (GDNF)). GFRα1 is shown in a *blue loop ribbon*, and GDNF is shown in a *salmon loop ribbon*. The residues mutated in this study are labeled *red*. This figure and Figs. 3–5 were made using PyMol (32).

However, most significant is our direct experimental evidence for the probable RET-binding interface. Arg-190, Lys-194, Arg-197, Gln-198, Lys-202, Arg-257, Arg-259, Glu-323, and Asp-324 are all on the surface of GFRα1 (Fig. 3*D*), not in the GDNF·GFRα1 interface, yet mutation reduces RET phosphorylation by a factor of 3 or more (Table 3 and Fig. 1*B*). Thus, these residues interact with RET. The effect of the E323A/D324A and R257A/R259A mutants is consistent with earlier predictions (13). The slightly greater effect of the R190A/R197A, K194A, and Q198A/K202A mutants (Table 3 and Fig. 1*B*) suggest that the RET-binding and heparin-binding interfaces (Fig. 3, *A* and *D*) may overlap, as mentioned above. Binding studies were consistent with these results.[5]

Structural and Signaling Differences between $GDNF_2$·$GFR\alpha1_2$ and $ARTN_2$·$GFR\alpha3_2$ Complexes—The $GDNF_2$·$GFR\alpha1_2$ and $ARTN_2$·$GFR\alpha3_2$ (Protein Data Bank code 2GH0 (13)) structures are similar in three respects: the GFL fingertips bind their respective co-receptor through the center of the triangular helix spiral (Fig. 4*A*); both contain the same Arg-$171^{GFR\alpha1}$-Glu-61^{GDNF}-Arg-$224^{GFR\alpha1}$ ion triple (Arg-179-Glu-143-Arg-233 in ARTN·GFRα3); and the GFRα1 and GFRα3 structures are highly similar (root mean square deviation of 0.89 Å for 166 Cα atoms). Despite the above, the complexes differ in three important ways.

First, the approach of the ligand fingers at the ligand-co-receptor interface is different (Fig. 4*A*). With respect to GDNF, the ARTN fingers twist about their longitudinal axis and turn around a vertical axis (Fig. 4*A*) emanating out of the GFRα triangular helix spiral by about 20°.

[5] J. M. Jurvansuu, and M. M. Bespalov, unpublished results.

Second, there are differences in the core region of the ligand-co-receptor binding interface. As mentioned above, GFRα1 N162 buttresses the Arg-Glu-Arg ion triple (Fig. 2*C*), and the GFRα1 N162A mutant shows no stimulation of RET phosphorylation (Table 3). The equivalent GFRα3 Thr-170 makes no interactions at all. The changes in hydrophobic packing by the GFRαs around GDNF Tyr-120 *versus* ARTN Trp-205 are equally as important. As can be seen (Fig. 4*B*), the GFRα3 pocket is wider and not as deep, consistent with it binding Trp, not Tyr. The difference in the shape of the hydrophobic pocket is due to the Ile-$175^{GFR\alpha1}$ → $Gly^{GFR\alpha3}$ and Val-$230^{GFR\alpha1}$ → $Ala^{GFR\alpha3}$ changes. These changes are important in determining the specificity. Such changes would lead to GDNF binding poorly to GFRα3 and vice versa (Fig. 4*B*). Consistent with this,

TABLE 2

Interface contact residues within 4 Å

We searched for residues in GFRα1 that were within 4 Å of residues in GDNF.

GDNF	GFRα1
Lys-60	Lys-155
Glu-61	Ala-158, Asn-162, Arg-171, Arg-224
Glu-62	Lys-159, Asn-162 (Glu-62[a])
Ile-64	Leu-163
Asp-108	Lys-168[b]
Asp-109	Lys-168[b], Lys-169
Asp-110	Ser-172 (Asp-110[a])
Leu-111	Asn-162, Lys-168
Ser-112	Asn-162 (Ser-112[a]), Arg-171, Ser-172, Ile-175
Leu-114	Arg-224
Leu-118	Glu-223
Tyr-120	Ile-175, Gln-227,[a] Val-230 and Arg-171,[b] Tyr-174,[b] Thr-228[b]
Ile-122	Ile-175, Thr-176
Arg-124	Thr-176

[a] Through backbone.
[b] Through water.

the Ile-175$^{GFR\alpha1}$ → Gly mutation alone reduces GDNF stimulation of GFRα1-RET more than 20-fold (Table 3).

Third, the ARTN and GDNF monomer finger loop regions, relative to the aligned helical heel, are inclined by about 20° in comparison with each other (Fig. 4*C*). Consequently, the dimer bend angle difference between bound $GDNF_2$ and $ARTN_2$ is 44°, because the GDNF homodimer is bent and the ARTN homodimer is planar. The large change in bend angle between $GDNF_2$ and $ARTN_2$ makes it impossible to superimpose the structures globally. The root mean square deviation/Cα between $GDNF_2$ and $ARTN_2$ homodimers is over 5 Å. Unbound GDNF (25) and ARTN (36) also have a similar difference in their bend angle; the difference is thus not due to co-receptor binding. In addition, another $(GDNF{\cdot}GFR\alpha1)_2$ crystal structure grown in the absence of SOS with therefore

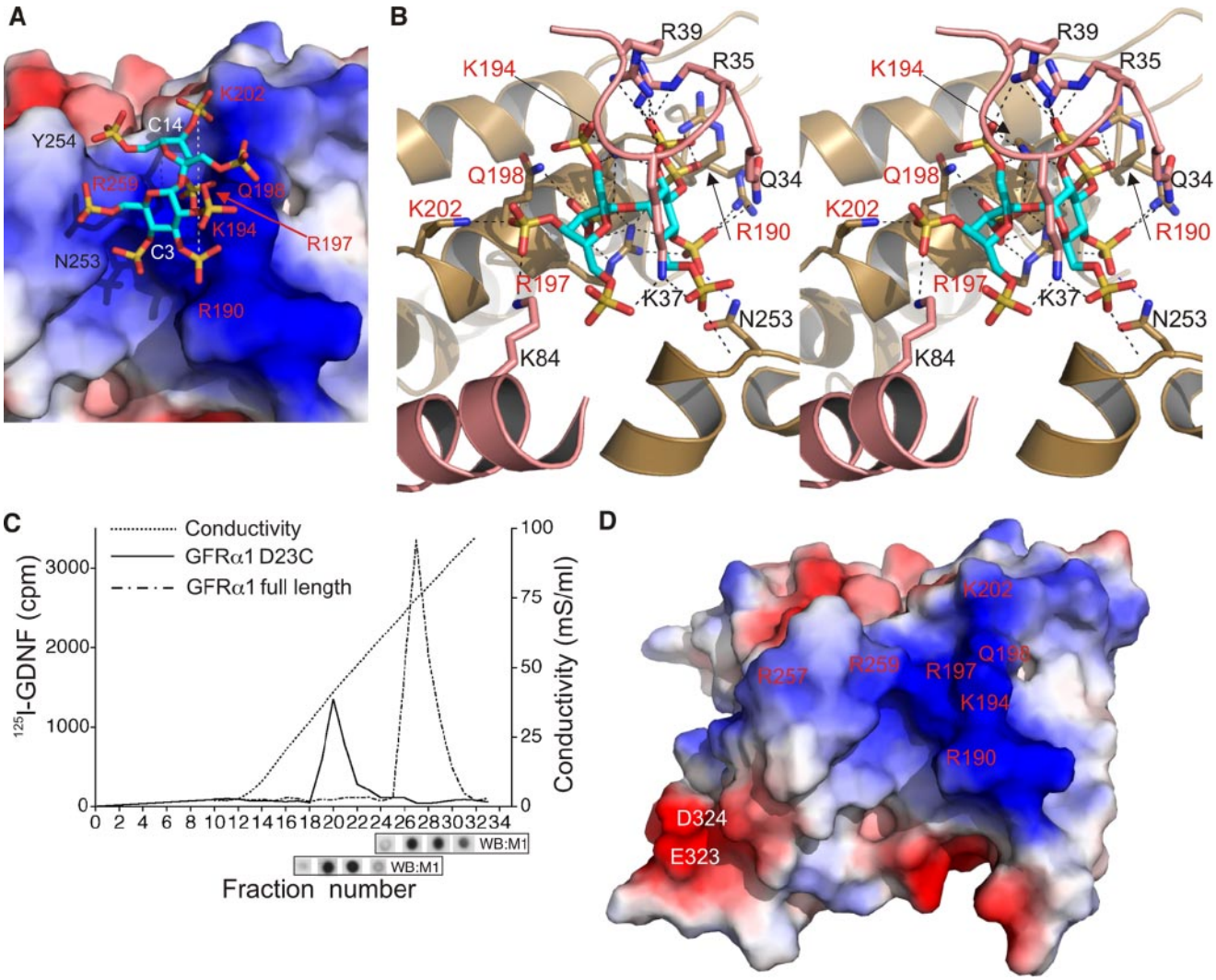

FIGURE 3. **Heparin and SOS binding to GFRα1 D23C and GDNF.** *A*, close-up view of the GFRα1-SOS interface, with GFRα1 as a surface representation *colored* by charge, and the interacting residues were *labeled*. The SOS is shown in *sticks color-coded* as in Fig. 2*A*. The *dashed line* represents the spacing between the two 2-*O*-sulfates of the SOS (10.4 Å) that interact with the Arg-190 to Lys-202 region of GFRα1. Arg-197, beneath the SOS, is marked with an *arrow*. The residues mutated in this study have *red labels*. *B*, stereo view of the interaction between SOS, GFRα1, and GDNF. The GFRα1 is in a *sand ribbon*, the GDNF (from the neighboring complex in the crystal) is in *salmon*, and the side chains that interact with the SOS are shown as *sticks*. The mutated GFRα1 residues have *red labels*. Hydrogen bonds are shown as *black dashed lines*. The *arrows* point to the branch point between the two conformations of Arg-190 and to Lys-194, hidden under GDNF. *C*, comparison of full-length GFRα1 and truncated GFRα1 D23C binding to the heparin column. Fractions were assayed for ^{125}I-GDNF binding by scintillation proximity assay. GFRα1 D23C and the full-length GFRα1 elute at about 0.5–0.6 M NaCl and 1.0–1.2 M NaCl, respectively. The *inset* immunoblot, using anti-FLAG antibody, shows that GFRα1 D23C elutes in fractions 20–22, and full-length GFRα1 elutes in fractions 26–28, so ^{125}I-GDNF binding correlates with GFRα1. *D*, proposed RET binding surface *colored* by charge. The electrostatic surface view of the GFRα1 D23 is shown. The RET-interacting residues mutated in this study are labeled in *red*, except for Glu-323 and Asp-324, which have *white labels*. The orientation is as in *A*.

TABLE 3

Stimulation of RET phosphorylation by GDNF

Each ELISA experiment was done in at least triplicate, and each experiment was repeated at least twice. The percentage stimulation is calculated as follows, stimulation = $100 \times ((\text{mutant}^{+GDNF} - \text{mut}^{-GDNF})/(\text{wild type}^{+GDNF} - \text{wild type}^{-GDNF}))$.

Mutant	GFRα3 equivalent	Stimulation with respect to wild type ± S.E.
		%
Wild type		100
GDNF·GFRα1 interface		
K159A	Met-167	59 ± 10
N162A	Thr-170	3 ± 8
K168A	Asp-176	35 ± 4
I175G	Gly-183	3 ± 2
SOS-binding region		
R190A/R197A	Lys-194/Arg-201	30 ± 8
K194A	Ala-198	28 ± 3
Q198A/K202A	Ser-202/Lys-206	36 ± 4
R257A/R259A	Arg-262/Arg-264	28 ± 7
Potential RET binding		
D164A	Asn-172	51 ± 1
E323A/D324A	Glu-326/Glu-327	37 ± 8
Others		
R217E	Ala-221	71 ± 36
R240A	Ala-245	92 ± 30

different crystal packing,[6] has a similar bend angle to the $(GDNF{\cdot}GFR\alpha1)_2$ complex described here.

These differences mean that the quaternary structures of the two complexes are dissimilar (Fig. 2, *A* and *B*). This, we believe, explains how GFLs cause differential signaling through RET, although RET phosphorylation is unchanged (37). The different bend angles could change the presentation of the RET tyrosine kinase domains on the inside of the cell and thus alter the surfaces that are available for adaptor proteins to dock (see "Discussion").

We therefore decided to reinvestigate whether there were signaling differences between GDNF and ARTN, although earlier reports showed no difference in RET phosphorylation nor in how fast phosphorylation occurs (37). Our results show that GDNF activates the MAPK pathway faster than ARTN, as measured by our luciferase readout system (Fig. 4*D*).

SOS as a Model for Heparin—Previous studies showed that 2-*O*-sulfation was important in binding of heparin to GDNF (38) and in biological assays of function, such as ureteric bud branching in developing kidneys (39). Davies *et al.* (39) also showed that the minimum length of heparin capable of inhibition was about 12 saccharides long.

Our work may help explain why. The distances between nearest neighbor 2-*O*-sulfates in heparin are about 9–12 Å, similar to the 10.4-Å spacing between the SOS C3 and C14 sulfates that bind GFRα1 (Fig. 3*A*). It was therefore easy to model a heparin pentasaccharide into the SOS-binding region with the 2-*O*-sulfates in a similar orientation to those of SOS (Fig. 5). Since mutations in this region affect RET phosphorylation (Table 3), exogenous heparin could prevent RET binding to the $GDNF_2{\cdot}GFR\alpha1_2$ complex and thus inhibit RET phosphorylation and signaling. Such inhibition would depend on both length and 2-*O*-sulfation, as has been observed (21, 39).

[6] Parkash, unpublished results.

DISCUSSION

A Putative RET Binding Surface—Wang and co-workers (13) proposed that a conserved charged surface on GFRα3, including Asp-164, Lys-202, Arg-257, Arg-259, Glu-323, and Asp-324 (GFRα1 numbering), bound RET. However, they showed no experiments to demonstrate that this was so. Our mutagenesis and RET phosphorylation ELISA assays, therefore, are the first experimental demonstration of a putative RET-binding interface on GFRα1 (Fig. 3*D*). Of the proposed residues, Asp-164 is not in the RET interface (Table 3), but the other ones are (Fig. 3*D*). In addition, we have also identified other positively charged surface-exposed residues near Lys-202 as being in the RET interface: Arg-190, Lys-194, and Arg-197 (Fig. 3*D*). The RET interface thus extends the full length of the exposed surface of both domains 2 and 3 (Fig. 3*D*). The positively charged region on domain 2 could interact with the negatively charged RET cysteine-rich domain (residues 516–636), consistent with cross-linking studies (40). Furthermore, both this region and the RET cysteine-rich domain are close to the membrane. The other part of the putative RET interface, at the tip of D3 near Glu-323/Asp-324 and thus farther away from the cell surface (13), may interact with the RET cadherin-like domains (41).

RET Activation Is a Result of Proximity—The structure of the RET tyrosine kinase domain does not change upon phosphorylation, and the nonphosphorylated kinase domain is active (42). Lack of phosphorylation of the "A-loop" structure (43) interferes with neither ATP nor substrate binding (42), unlike in most receptor tyrosine kinases (43). The RET tyrosine kinase thus appears to be always active, and all GFLs appear to induce the same level of RET phosphorylation (37). Nonetheless, a recent report suggested that NRTN and GDNF activate MAPK and phospholipase C-γ differently (44). In addition, our MAPK luciferase assay indicates a higher level signaling through RET by GDNF than ARTN (Fig. 4*D*).

Differences in the binding interface and in the GFL bend angle (Fig. 4, *A* and *C*) may explain the differential activation. They change the quaternary arrangement of the rigid GFRαs in the heterotetramer complex (Fig. 2, *A* and *B*). For instance, the distance between the Glu-323 Cαs on GFRα1 in $GDNF_2{\cdot}GFR\alpha1_2$ is 115 Å, whereas the equivalent distance in $ARTN_2{\cdot}GFR\alpha3_2$ is 135 Å. Since the RET interaction interface seems to be conserved in GFRαs, the arrangement of the extracellular RET domains must change. This might affect the positioning of the RETs with respect to each other on the inside of the membrane and thus which tyrosines are available to bind downstream effectors (45). Such changes could lead to different downstream signaling complexes and the variable signaling observed (44) (Fig. 4*D*). It is, of course, possible that the GFL·GFRα complexes all adopt the same conformation upon binding RET, but this seems unlikely, since all of the ARTN structures solved so far have been essentially flat (13, 36), whereas all of the GDNF structures have been bent (25) (Fig. 4*C*). The variable presentation suggested above might also explain why the GFRα homologue Gas1, which does not require a GFL to signal through RET, activates targets different from those activated by $GDNF_2{\cdot}GFR\alpha1_2$ (46).

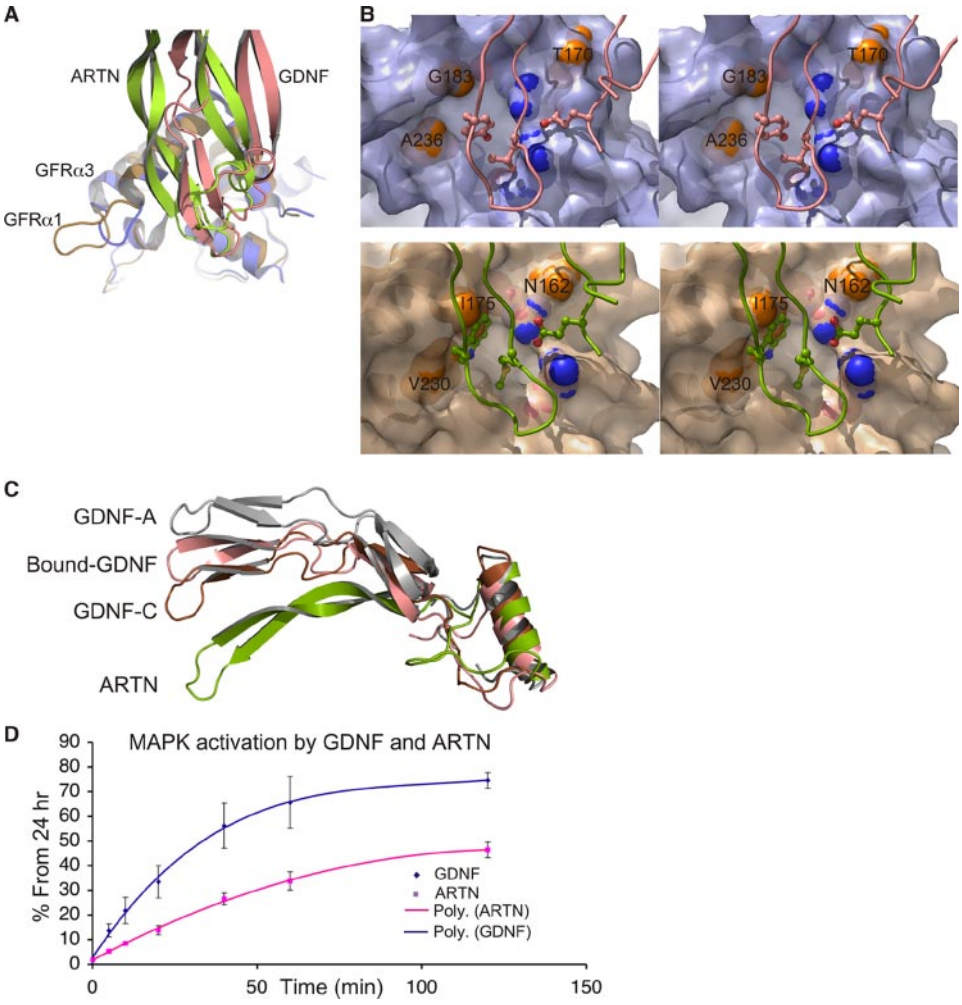

FIGURE 4. **Comparison of the $GDNF_2$·$GFR\alpha1_2$ and $ARTN_2$·$GFR\alpha3_2$ complexes.** *A*, superposition of the GFL·GFRα monomers to show the difference in approach between GDNF and ARTN viewed from above looking into the triangular helix spiral. The GFRαs were superimposed. *Sand*, GFRα1; *slate*, GFRα3; *salmon*, GDNF; *pea green*, ARTN. This view emphasizes the difference in rotation between GDNF and ARTN finger loops *above* the *triangle* of helices. *B*, close-up of the "cross-talk" ligand-co-receptor complex interfaces in stereo. In the *top panel*, the GFRα3 in a partially transparent surface representation is positioned *below* GDNF, and GFRα1 is shown similarly *below* ARTN in the *bottom panel*. The GFRα1, GFRα3, GDNF, and ARTN are in same *color* and *alignment* as in *A*. The key differences between GFRα1 and GFRα3 are shown in *orange balls*, and the two arginines of the ion triple are in *balls* with carbon (*sand*), oxygen (*red*), and nitrogen (*blue*). The key GDNF (Glu-61, Leu-114, and Tyr-120) and ARTN (Glu-143, Met-199, and Trp-205) residues are shown as *ball-and-stick models*. *C*, the ligand bend angle difference. The conserved ligand monomer heel structures were aligned to show the relative inclination of the finger loops. Two conformations of GDNF (25) (Protein Data Bank code 1AGQ; chain A in *steel gray* and chain C in *brown*), GDNF (*salmon*) from our complex structure, and ARTN (*pea green*) from Wang *et al.* (13) are shown. For a clear view, only heel and finger 2 are shown for all the GDNF and ARTN monomers. *D*, kinetics of MAPK activation by GDNF or ARTN monitored by luciferase activity. The luciferase activity value after a 24-h incubation with corresponding neurotrophic factors is normalized to 100%.

The Role of Heparan Sulfate in GDNF Signaling—Alfano *et al.* (21) showed that heparin binds chiefly to the N-terminal 40 residues of GDNF, in particular residues 24–39 (supplemental Fig. 1*D*).[7] Although our GDNF structure is truncated at residue 34, it nonetheless contains part of this proposed heparin-binding site, and the heparin mimic SOS binds GDNF. The GDNF residues that interact are Arg-35, Lys-37, and Arg-39 (Fig. 3*B*) and possibly Lys-84 in the GDNF heel region.

Our structure thus supports the biochemical data, and it further explains how heparin can inhibit RET signaling even after the "heparin-binding sequence" in GDNF (residues 24–39) is removed (21). We believe that heparin inhibits RET signaling by binding to the Arg-190 to Lys-202 patch on helix α3 in GFRα1 D2 (Fig. 3*A*). The biochemically identified heparin interactions with the N terminus of GDNF and with GFRα1 D1 should thus have different biological roles. One possibility is discussed below.

In Trans Signaling and Cell Adhesion—Very recent work has shown that, in the absence of RET, the $GDNF_2$·$GFR\alpha1_2$ complex causes signaling at the synapse during development. Ledda *et al.* (20) suggested that $GDNF_2$·$GFR\alpha1_2$ could act as an adhesin and play an active role in synapse induction. The structural arrangement in the crystal suggests that this may be due to heparin-linked oligomerization of the $GDNF_2$·$GFR\alpha1_2$ tetramers between cells. There are three heparin-binding regions: the N terminus (residues 24–39) and the "heel" of GDNF (21, 36) (Fig. 3*B*), GFRα1 D1 (Fig. 3*C*), and the GFRα1 D2 Arg-190 to Lys-202 region (Fig. 3*A*).

In our crystal structure, SOS links a $GDNF_2$·$GFR\alpha1_2$ tetramer to its crystallographic neighbor by interacting on one side with the N terminus and heel region of GDNF and on the other side with GFRα1 D2 helix α3 (Fig. 3*B*). SOS thus mediates "dimer-of-heterotetramer" formation in the crystal, and we believe that heparin might also cross-link $GDNF_2$·$GFR\alpha1_2$ tetramers. Such cross-linking could extend from cell to cell.

Although such a model is highly speculative, it is consistent with the observed $GDNF_2$·$GFR\alpha1_2$-induced cell adhesion and synapse formation (20). Finally, our model also suggests that this should occur for $GDNF_2$·$GFR\alpha1_2$ and $NRTN_2$·$GFR\alpha2_2$ but not for $ARTN_2$·$GFR\alpha3_2$ and $PSPN_2$·$GFR\alpha4_2$. GFRα3 has three changes in the domain 2 heparin-binding patch (R190H, K194A, and Q198S (GFRα1 numbering) (supplemental Fig. 1*D*)), whereas PSPN lacks the N-terminal heparin-binding region and does not bind heparin (47). Without heparin binding, the multimerization required for GFL·heparin·GFRα-mediated cell adhesion would not occur.

Conclusion—Our studies of the $GDNF_2$·$GFR\alpha1_2$ complex suggest how ligand binding, specificity, and affinity are related in this important neurotrophic factor-receptor system. They

[7] H. Virtanen, M. M. Bespalov, Y. A. Sidorova, P. Runeberg-Roos, and M. Saarma, unpublished results.

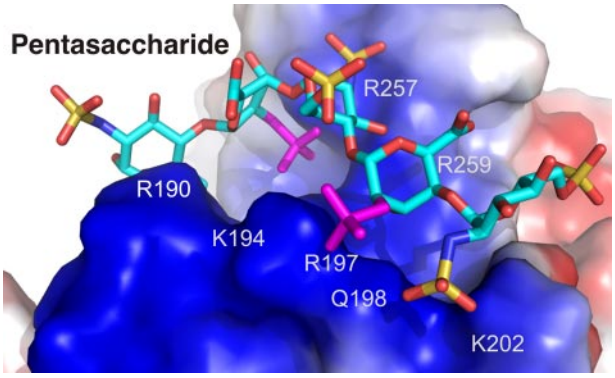

FIGURE 5. **Heparin modeling.** Shown is modeling of heparin (pentasaccharide, Protein Data Bank code 1AXM (48); chain G) onto GFRα1 to show the possible interaction of heparin with GFRα1. The 2-*O*-sulfates of the heparin oligomer were aligned to the two interacting sulfate groups of SOS (root mean square deviation of 0.21 Å), which bind positively charged residues of GFRα1 (residues 190–202) in the $GDNF_2$·$GFR\alpha1_2$·SOS_2 structure (Fig. 3*A*). The pentasaccharide is shown as *sticks*, *color-coded* as SOS in Fig. 2*A*. The GFRα1 surface is *colored* by charge. 2-*O*-Sulfates are shown in *magenta*.

also provide an intriguing model of how *in trans* signaling may occur. The work provides a structural basis for design of GDNF agonists for use in diseases such as Parkinson syndrome.

Acknowledgments—We thank Hanna Valo and Dr. Tero Pihlajamaa for preparation and analysis of these complexes and Professor Jari Ylänne for help with data collection. We acknowledge the European Synchrotron Radiation Facility for beam time and Dr. Joanna Timmins for assistance at ID14-EH2. Beam time was made available at the ESRF under EU Contract HPRI-CT-1999-00022.

REFERENCES

1. Lin, L.-F., Doherty, D. H., Lile, J. D., Bektesh, S., and Collins, F. (1993) *Science* **260,** 1130–1132
2. Airaksinen, M. S., and Saarma, M. (2002) *Nat. Rev. Neurosci.* **3,** 383–394
3. Shults, C. W., Kimber, T., and Martin, D. (1996) *Neuroreport* **7,** 627–631
4. Yasuhara, T., Shingo, T., and Date, I. (2007) *Acta Med. Okayama* **61,** 51–56
5. Kotzbauer, P. T., Lampe, P. A., Heuckeroth, R. O., Golden, J. P., Creedon, D. J., Johnson, E. M., Jr., and Milbrandt, J. (1996) *Nature* **384,** 467–470
6. Baloh, R. H., Tansey, M. G., Lampe, P. A., Fahrner, T. J., Enomoto, H., Simburger, K. S., Leitner, M. L., Araki, T., Johnson, E. M., Jr., and Milbrandt, J. (1998) *Neuron* **21,** 1291–1302
7. Milbrandt, J., de Sauvage, F. J., Fahrner, T. J., Baloh, R. H., Leitner, M. L., Tansey, M. G., Lampe, P. A., Heuckeroth, R. O., Kotzbauer, P. T., Simburger, K. S., Golden, J. P., Davies, J. A., Vejsada, R., Kato, A. C., Hynes, M., Sherman, D., Nishimura, M., Wang, L.-C., Vandlen, R., Moffat, B., Klein, R. D., Poulsen, K., Gray, C., Garces, A., Henderson, C. E., Phillips, H. S., and Johnson, E. M., Jr. (1998) *Neuron* **20,** 245–253
8. Takahashi, M., and Cooper, G. M. (1987) *Mol. Cell Biol.* **7,** 1378–1385
9. Lakhani, V. T., You, Y. N., and Wells, S. A. (2007) *Annu. Rev. Med.* **58,** 253–265
10. Plaza-Menacho, I., Burzynski, G. M., de Groot, J. W., Eggen, B. J., and Hofstra, R. M. (2006) *Trends Genet.* **22,** 627–636
11. Airaksinen, M. S., Titievsky, A., and Saarma, M. (1999) *Mol. Cell Neurosci.* **13,** 313–325
12. Lindahl, M., Poteryaev, D., Yu, L., Arumäe, U., Timmusk, T., Bongarzone, I., Aiello, A., Pierotti, M. A., Airaksinen, M. S., and Saarma, M. (2001) *J. Biol. Chem.* **276,** 9344–9351
13. Wang, X., Baloh, R. H., Milbrandt, J., and Garcia, K. C. (2006) *Structure* **14,** 1083–1092
14. Leppänen, V.-M., Bespalov, M. M., Runeberg-Roos, P., Puurand, ü., Merits, A., Saarma, M., and Goldman, A. (2004) *EMBO J.* **23,** 1452–1462
15. Scott, R. P., and Ibáñez, C. F. (2001) *J. Biol. Chem.* **276,** 1450–1458
16. Virtanen, H., Yang, J., Bespalov, M. M., Hiltunen, J. O., Leppänen, V. M., Kalkkinen, N., Goldman, A., Saarma, M., and Runeberg-Roos, P. (2005) *Biochem. J.* **387,** 817–824
17. Jing, S., Wen, D., Yu, Y., Holst, P. L., Luo, Y., Fang, M., Tamir, R., Antonio, L., Hu, Z., Cupples, R., Louis, J.-C., Hu, S., Altrock, B. W., and Fox, G. M. (1996) *Cell* **85,** 1113–1124
18. Schlee, S., Carmillo, P., and Whitty, A. (2006) *Nat. Chem. Biol.* **2,** 636–644
19. Paratcha, G., Ledda, F., and Ibáñez, C. F. (2003) *Cell* **113,** 867–879
20. Ledda, F., Paratcha, G., Sandoval-Guzmán, T., and Ibáñez, C. F. (2007) *Nat. Neurosci.* **10,** 293–300
21. Alfano, I., Vora, P., Mummery, R. S., Mulloy, B., and Rider, C. C. (2007) *Biochem. J.* **404,** 131–140
22. Keinänen, K., Jouppila, A., and Kuusinen, A. (1998) *Biochem. J.* **330,** 1461–1467
23. Eketjäll, S., Fainzilber, M., Murray-Rust, J., and Ibáñez, C. F. (1999) *EMBO J.* **18,** 5901–5910
24. Kabsch, W. (1993) *J. Appl. Crystallogr.* **26,** 795–800
25. Eigenbrot, C., and Gerber, N. (1997) *Nat. Struct. Biol.* **4,** 435–438
26. Read, R. J. (2001) *Acta Crystallogr. Sect. D Biol. Crystallogr.* **57,** 1373–1382
27. Morris, R. J., Perrakis, A., and Lamzin, V. S. (2002) *Acta Crystallogr. Sect. D Biol. Crystallogr.* **58,** 968–975
28. Murshudov, G. N., Vagin, A. A., Lebedev, A., Wilson, K. S., and Dodson, E. J. (1999) *Acta Crystallogr. Sect. D Biol. Crystallogr.* **55,** 247–255
29. Emsley, P., and Cowtan, K. (2004) *Acta Crystallogr. Sect. D Biol. Crystallogr.* **60,** 2126–2132
30. Laskowski, R. A., MacArthur, M. W., Moss, D. S., and Thornton, J. M. (1993) *J. Appl. Crystallogr.* **26,** 283–291
31. Schüttelkopf, A. W., and van Aalten, D. M. F. (2004) *Acta Crystallogr. Sect. D Biol. Crystallogr.* **60,** 1355–1363
32. DeLano, W. L. (2002) PyMol, DeLano Scientific LLC, Palo Alto, CA
33. Chenna, R., Sugawara, H., Koike, T., Lopez, R., Gibson, T. J., Higgins, D. G., and Thompson, J. D. (2003) *Nucleic Acids Res.* **31,** 3497–3500
34. Fraternali, F., and Cavallo, L. (2002) *Nucleic Acids Res.* **30,** 2950–2960
35. Barnett, M. W., Fisher, C. E., Perona-Wright, G., and Davies, J. A. (2002) *J. Cell Sci.* **115,** 4495–4503
36. Silvian, L., Jin, P., Carmillo, P., Boriack-Sjodin, P. A., Pelletier, C., Rushe, M., Gong, B., Sah, D., Pepinsky, B., and Rossomando, A. (2006) *Biochemistry* **45,** 6801–6812
37. Coulpier, M., Anders, J., and Ibáñez, C. F. (2002) *J. Biol. Chem.* **277,** 1991–1999
38. Rickard, S. M., Mummery, R. S., Mulloy, B., and Rider, C. C. (2003) *Glycobiology* **13,** 419–426
39. Davies, J. A., Yates, E. A., and Turnbull, J. E. (2003) *Growth Factors* **21,** 109–119
40. Amoresano, A., Incoronato, M., Monti, G., Pucci, P., de Franciscis, V., and Cerchia, L. (2005) *Cell. Signal.* **17,** 717–727
41. Kjær, S., and Ibáñez, C. F. (2003) *J. Biol. Chem.* **278,** 47898–47904
42. Knowles, P. P., Murray-Rust, J., Kjær, S., Scott, R. P., Hanrahan, S., Santoro, M., Ibáñez, C. F., and McDonald, N. Q. (2006) *J. Biol. Chem.* **281,** 33577–33587
43. Schlessinger, J. (2003) *Science* **300,** 750–752
44. Lee, R. H. K., Wong, W. L., Chan, C. H., and Chan, S. Y. (2006) *J. Neurosci. Res.* **83,** 80–90
45. Arighi, E., Borrello, M. G., and Sariola, H. (2005) *Cytokine Growth Factor Rev.* **16,** 441–467
46. Cabrera, J. R., Sanchez-Pulido, L., Rojas, A. M., Valencia, A., Manes, S., Naranjo, J. R., and Mellström, B. (2006) *J. Biol. Chem.* **281,** 14330–14339
47. Baloh, R. H., Tansey, M. G., Johnson, E. M., Jr., and Milbrandt, J. (2000) *J. Biol. Chem.* **275,** 3412–3420
48. DiGabriele, A. D., Lax, I., Chen, D. I., Svahn, C. M., Jaye, M., Schlessinger, J., and Hendrickson, W. A. (1998) *Nature* **393,** 812–817